

# Exploiting Multipath Echoes with Capon Method for High-Resolution Ultra-Wideband Radar Imaging using a Single Omni-Directional Antenna

Takuya Sakamoto\*, Toru Sato,  
Graduate School of Informatics  
Kyoto University  
Yoshida-Honmachi, Sakyo-ku  
Kyoto 606-8501, Japan

**Abstract**—A high-resolution imaging algorithm is proposed that uses ultra-wideband monostatic radar with only a single omni-directional antenna. With such a simple system, conventional radars can only measure distances between target and antenna. In a multipath environment, however, we can also use multipath echoes that can be separated from the actual echo in the time domain, if the pulse width is shorter than the difference in path lengths. Under this condition, assuming imaginary mirror images of the actual antenna, a radar image can be produced using delay-and-sum migration. However, images generated using DAS migration and imaginary-mirror antennas suffer from insufficient resolution. The proposed method uses multipath Green functions and Capon method to overcome limitations of conventional method. We apply the proposed method to numerical data and compare the imaging results with those from conventional methods. Results from applications demonstrate that the proposed method outperforms conventional imaging methods.

## I. INTRODUCTION

Ultra-wideband (UWB) radar imaging has a remarkably high range resolution, resulting in numerous important applications ranging from landmine detection to security monitoring. In an indoor environment, however, multipath echoes must be properly dealt with for accurate imaging. One option is suppressing multipath effects to generate interference-free images as performed by Arriba-Ruiz et al. [1]. The other option is exploiting such effects to improve imaging capabilities.

A series of studies exploiting multipath echoes in UWB radar imaging were initiated by the authors in 2010 [2], [3], and enabled imaging of targets in blind spots using multipath echoes. Sakamoto and Sato developed an accurate imaging algorithm to locate a point target using only a single omni-directional antenna [4], [5]. These studies assumed prior information of the multipath environment, whereas Kidera et al. proposed a two-step method in which the multipath environment is estimated first; the multipath is then exploited to generate a more accurate image [6]. These studies have been advanced by Setlur et al. [7], [8], [9], Gennarelli and Soldovieri [10], Smith and Mobasseri [11], and reviewed by Leigsnering [12].

We describe an extension of the single-antenna imaging concept [4], [5] that further improves its resolution. When con-

ventional radar signal processing is used, a radar with a single omni-directional antenna can provide only range information, i.e. the distance to the target. In contrast, by taking into account the multipath environment, we can assume imaginary-mirror antennas to form a quasi-array, with which even conventional methods such as delay-and-sum (DAS) migration can generate images. To improve imaging capabilities, a singular value decomposition (SVD)-based algorithm was developed [4], [5] that uses a noise subspace spanned by vectors corresponding to small singular values. Thus, it is necessary to know the number of echoes (or the dimension of the signal subspace). In practice, this is difficult to ascertain in a multipath environment because the number of multipath echoes is much larger than the number of actual targets. We propose a new method using the Capon method that does not require knowing the number of echoes. We use a steering vector formed using the Green functions that include multipath effects. The proposed method is applied to numerical data in a simulation, and compared with conventional imaging methods.

## II. SYSTEM MODEL

The system model for this study is a two-dimensional system (Figure 1), using transverse magnetic waves. We assume a monostatic radar composed of a single omni-directional antenna used as the transmitting antenna Tx as well as the receiving antenna Rx, a metallic plate W, and a target (or targets) P. The plate W and antenna are situated on the  $x$ - and  $y$ -axes, respectively. The positions for Tx/Rx, which are fixed and non-scanning, are set at  $\mathbf{r}_A = (0, y_A)$ . The figure also shows the imaginary mirror image of the actual antenna located at  $\bar{\mathbf{r}}_A(0, -y_A)$ . The dashed lines in the figure are the propagation paths considered in our analysis.

The propagation in this system model is described using the Green function. The transmitted signal is  $s_T(t)$ , where  $t$  is time. We assume that the distance between antennas Tx/Rx and plate W is known. This assumption is not unrealistic as the distance can easily be measured in advance by detecting the strong reflection echo from the plate. The direct wave  $s_D(t)$  that propagates without scattering from Tx to Rx, and the reflected wave  $s_W(t)$  from plate W are measured and stored

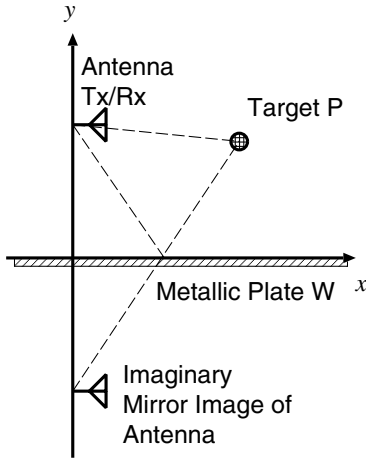


Fig. 1. System model of a multipath scattering UWB radar.

in memory prior to actual measurements. These waveforms,  $s_D(t)$  and  $s_W(t)$ , are subtracted from the received signal  $s_0(t)$  yielding  $s(t) = s_0(t) - s_D(t) - s_W(t)$ .

The paths of the four dominant components in signal  $s(t)$  are:

- $s_1(t)$  Tx-P-Rx,
- $s_2'(t)$  Tx-P-W-Rx,
- $s_2''(t)$  Tx-W-P-Rx, and
- $s_3(t)$  Tx-W-P-W-Rx,

where the paths corresponding to  $s_2'(t)$  and  $s_2''(t)$  are traversed in opposite directions. As a consequence, these echoes cannot be separated if the system satisfies the condition appropriate to the Lorentz reciprocal theorem. Hereafter, by introducing  $s_2(t) = s_2'(t) + s_2''(t)$ , only three paths are considered. Additionally, note that this model ignores higher-order multiple scattering components.

Next, we introduce  $G(\omega, \mathbf{r}, \mathbf{r}')$ , the Green function including multipath scattering effects associated with propagation through a medium from point  $\mathbf{r}$  to point  $\mathbf{r}'$ , expressed as

$$G(\omega, \mathbf{r}, \mathbf{r}') = G_0(\omega, \mathbf{r}, \mathbf{r}') - G_0(\omega, \bar{\mathbf{r}}, \mathbf{r}') \quad (1)$$

where  $\omega$  is an angular frequency, and  $\bar{\mathbf{r}}$  is the point mirror symmetric with  $\mathbf{r}$  about the  $x$ -axis. The second term on the right-hand side of Eq. (1) has a negative sign because reflection from the metallic plate causes a  $\pi$  rad phase shift. The Green function for a 2-dimensional scalar wave  $G_0$  is expressed as

$$G_0(\omega, \mathbf{r}, \mathbf{r}') = \frac{j}{4} H^{(2)}\left(\frac{\omega}{c} |\mathbf{r} - \mathbf{r}'|\right), \quad (2)$$

where  $c$  is the speed of the radio wave,  $H^{(2)}$  a Hankel function of the second kind, and  $\mathbf{r}$  and  $\mathbf{r}'$  are the positions of the ends of the propagation path.

Using  $S_T(\omega)$ , the Fourier transform of a transmitted signal  $s_T(t)$ , scattering by a point target can be modeled assuming

the Born approximation

$$\begin{aligned} S(\omega) &= \int \omega^2 C(\mathbf{r}') G(\omega, \mathbf{r}_A, \mathbf{r}') G(\omega, \mathbf{r}', \mathbf{r}_A) S_T(\omega) d\mathbf{r}' \\ &= \int \omega^2 C(\mathbf{r}') G^2(\omega, \mathbf{r}_A, \mathbf{r}') S_T(\omega) d\mathbf{r}', \end{aligned} \quad (3)$$

where  $\mathbf{r}$  is an observation point and  $C(\mathbf{r}')$  is contrast function defined as  $C(\mathbf{r}') = (\varepsilon(\mathbf{r}') - \varepsilon_0(\mathbf{r}'))/\varepsilon_0(\mathbf{r}')$  using the relative permittivity of a target  $\varepsilon(\mathbf{r}')$  and background medium  $\varepsilon_0(\mathbf{r}')$  at position  $\mathbf{r}'$ .

### III. CONVENTIONAL DAS MIGRATION

DAS migration is a simple and well-known imaging algorithm. Let  $S(\omega)$  be the Fourier transform of the received signal  $s(t)$  after applying a matched filter  $S_T^*(\omega)$ . The DAS migration image is expressed as

$$\begin{aligned} I_{\text{DAS}}(\mathbf{r}) &= \left| \int S^*(\omega) G^2(\omega, \mathbf{r}_A, \mathbf{r}) d\omega \right|^2 \\ &= \left| \int S^*(\omega) \{ G_0^2(\omega, \mathbf{r}_A, \mathbf{r}) \right. \\ &\quad \left. - 2G_0(\omega, \mathbf{r}_A, \mathbf{r}) G_0(\omega, \bar{\mathbf{r}}_A, \mathbf{r}) + G_0^2(\omega, \bar{\mathbf{r}}_A, \mathbf{r}) \} d\omega \right|^2, \end{aligned} \quad (4)$$

For a single point target, the received signal  $S(\omega)$  is expressed approximately as

$$S(\omega) = \omega^2 G^2(\omega, \mathbf{r}_A, \mathbf{r}_P) |S_T(\omega)|^2, \quad (5)$$

disregarding constant terms. Substituting Eq. (5) into Eq. (4), we obtain

$$I_{\text{DAS}}(\mathbf{r}) = \left| \int \omega^2 |S_T(\omega)|^2 \{ G^*(\omega, \mathbf{r}_A, \mathbf{r}_P) G(\omega, \mathbf{r}_A, \mathbf{r}) \}^2 d\omega \right|^2, \quad (6)$$

which takes its maximum value when  $\mathbf{r} = \mathbf{r}_P$  because the integrand becomes real only in this case. This is the principle of DAS migration that gives a large value at the correct target positions.

We also consider Log-DAS migration, which is a modified version of DAS migration that produces an image by multiplying the three terms in Eq. (4) in the time domain, instead of adding them. That is, the produced image has non-zero pixels only when the three terms all have non-zero values. In this way, we can produce more accurate images as will be demonstrated in later sections.

### IV. PROPOSED METHOD

First, we apply the Fourier transform to the received signal to obtain its frequency-domain representation denoted  $S(\omega)$ . Let us define a  $D$ -dimensional complex vector  $\mathbf{x}_n$  as

$$\mathbf{x}_n = [ S(\omega_n), S(\omega_{n+1}) \cdots S(\omega_{n+D-1}) ]^T, \quad (7)$$

where  $\cdot^T$  denotes the matrix transpose operation, and  $\omega_n = \omega_0 + n\Delta\omega$  for  $n = 1, 2, \dots, N$ . We calculate a correlation matrix  $R_{xx}$  as

$$R_{xx} = \sum_{n=1}^{N-D+1} \mathbf{x}_n \mathbf{x}_n^H, \quad (8)$$

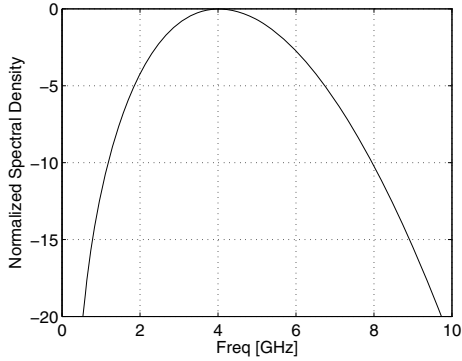


Fig. 2. Transmitted signal spectral density. The 3-dB frequency bandwidth is 3.8 GHz (2.3 GHz to 6.1 GHz).

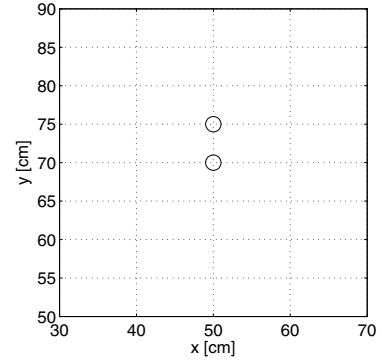


Fig. 3. Two metallic targets located at (50cm, 70cm) and (50cm, 75cm) spaced by 5 cm.

where  $\cdot^H$  denotes Hermitian conjugation. The image is obtained in the form of the Capon method as

$$I(\mathbf{r}) = \frac{1}{\mathbf{a}(\mathbf{r})^H \mathbf{R}_{xx}^{-1} \mathbf{a}(\mathbf{r})}, \quad (9)$$

where  $\mathbf{a}(\mathbf{r})$ , a steering vector composed of the multipath Green functions introduced in Section II, is defined as

$$\mathbf{a}(\mathbf{r}) = [G^2(\omega_1), G^2(\omega_2), \dots, G^2(\omega_D)]^T. \quad (10)$$

Here we have omitted arguments  $\mathbf{r}$  and  $\mathbf{r}_A$  for simplicity. Each Green function includes all four multipath propagation paths, as explained in Section II.

## V. COMPARISON OF IMAGING METHODS

We assume a single-antenna monostatic radar system as depicted in Fig. 1. The distance between the antenna and a metallic plate is  $y_A = 90\text{cm}$ . We transmit mono-cycle pulses from the antenna. The power spectrum of the transmitted signal is shown in Fig. 2. The center frequency is 4.0 GHz and the 3-dB bandwidth is 3.8 GHz, which corresponds to a range resolution of 3.9 cm.

Figure 3 shows the target positions located at  $\mathbf{r}_{P1} = (50.0\text{cm}, 70.0\text{cm})$  and  $\mathbf{r}_{P2} = (50.0\text{cm}, 75.0\text{cm})$ , respectively. Each target is a metallic wire of radius 0.1 cm. Note that the size of the targets as depicted in Fig. 3 does not represent the actual target size. The distance between the targets is 5.0 cm, which is larger than the range resolution 3.9 cm. However, the antenna is located at  $\mathbf{r}_A = (0.0\text{cm}, 90\text{cm})$  and the distance to each of the targets is 53.9 cm and 52.2 cm, meaning that the range difference is only 1.65 cm, i.e. is smaller than the range resolution. Additionally, the single omni-direction antenna does not have a cross-range resolution capability. Therefore, the assumed scenario is challenging for the setup of our radar system.

The received signal is calculated using the finite-difference time-domain (FDTD) method, with a 6-layered perfectly matched layer for absorbing boundaries and a grid size of 1.0 mm. Note that the absorbing condition is not satisfied at the ends of the metal plate, from which we receive small diffraction echoes. Figure 4 shows the received signal from

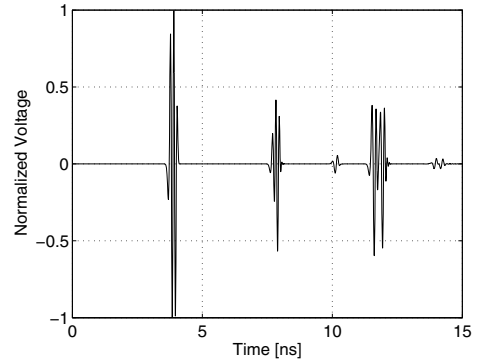


Fig. 4. Received signal using a monostatic UWB radar in a multipath environment.

the two targets. There are six dominant echoes forming three clusters corresponding to the three propagation paths (see Section II). Because the two targets are closely located to each other, some of the echoes overlap as seen in the figure. Unlike conventional array processing, there is no other information except this signal in our study. Thus, the imaging we deal with in this paper is not an easy task.

Figures 5, 6, and 7 show the images generated using the conventional DAS migration, Log-DAS migration, and proposed method. The image produced by the DAS migration has three echoes back-propagated to the region of interest, intersecting around the actual targets. However, the resultant image (Fig. 5) is not able to resolve the two targets. The Log-DAS migration produces a better image, from which at least we can see a clear bright region where the targets are actually located (see Fig. 6). Nonetheless, the image resolution is not high enough to show two distinct targets. In contrast, the proposed method can produce a high-resolution image (Fig. 7). We can clearly see two bright spots corresponding to the target positions. These results demonstrate that the imaging capability of the proposed method outperforms that of conventional ones.

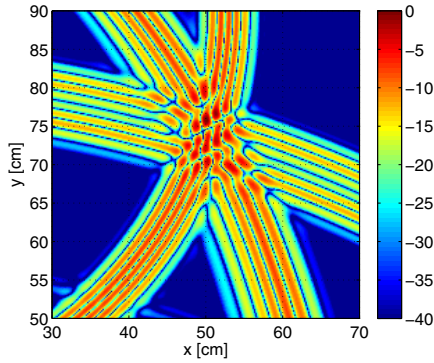


Fig. 5. Normalized image generated using the DAS migration (in decibels).

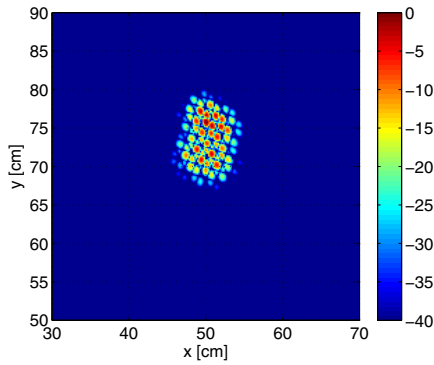


Fig. 6. Normalized image generated using the Log-DAS migration (in decibels).

## VI. CONCLUSION

We proposed a high-resolution UWB radar imaging method using the Capon method that exploits the multipath environment. The proposed method does not need multiple antennas or a scanning antenna; a fixed single omni-directional antenna and a known multipath environment is all that is required. The proposed method considers multipath propagation in calculating the Green function, leading to the unconventional

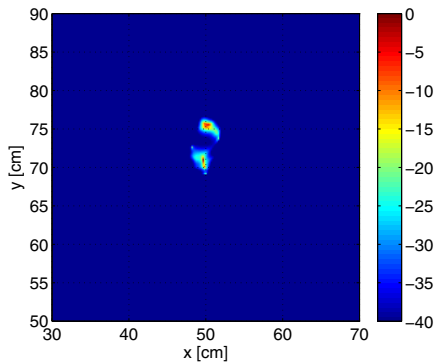


Fig. 7. Normalized image generated using the proposed method (in decibels).

steering vector used in the Capon method. The proposed method, together with conventional DAS migration and its modified method, Log-DAS migration, is applied to simulated data generated using the FDTD method. The imaging results clearly showed remarkable high-resolution capability for the proposed method that outperforms conventional DAS and Log-DAS migration methods. All conventional methods were not able to resolve the targets in the simulation. In contrast, the proposed method successfully separated the two targets spaced less than the pulse width of the radar signal in the range and cross-range directions. Although we assumed multipath echoes from a metallic plate, which is one of the simplest multipath conditions, our approach can be applied to any multipath environment.

## REFERENCES

- [1] I. de Arriba-Ruiz, F. M. Munoz-Ferreras, and F. Perez-Martinez, "Multipath mitigation techniques based on time reversal concept and super-resolution algorithms for inverse synthetic aperture radar imaging," *Radar, Sonar & Navigation, IET*, vol. 7, no. 4, pp. 413–421, 2013.
- [2] S. Fujita, T. Sakamoto, and T. Sato, "An accurate UWB radar imaging method using indoor multipath echoes for targets in shadow regions," *Proc. 2010 International Conference on Indoor Positioning and Indoor Navigation*, 2010.
- [3] S. Fujita, T. Sakamoto, and T. Sato, "2-Dimensional Accurate Imaging with UWB Radar Using Indoor Multipath Echoes for a Target in Shadow Regions," *IEICE Trans. Communications*, vol. E94-B, no. 8, pp. 2366–2374, 2011.
- [4] T. Sakamoto and T. Sato, "Image sharpening with waveform compensation for the frequency-domain DORT with a single-antenna UWB radar," *Proc. 2011 IEEE International Symposium on Antennas and Propagation*, pp. 484–487, 2011.
- [5] T. Sakamoto and T. Sato, "Performance Evaluation of the Frequency-Domain DORT Imaging Method with UWB Radar for a Finite-Sized Target," *Proc. 2011 IEEE International Geoscience and Remote Sensing Symposium*, pp. 51–54, 2011.
- [6] S. Kidera, T. Sakamoto, and T. Sato, "Extended Imaging Algorithm Based on Aperture Synthesis with Double Scattered Waves for UWB Radars," *IEEE Transactions on Geoscience and Remote Sensing*, vol. 49, no. 12, pp. 5128–5139, 2011.
- [7] P. Setlur, M. Amin, and F. Ahmad, "Multipath Model and Exploitation in Through-the-Wall and Urban Radar Sensing," *IEEE Transactions on Geoscience and Remote Sensing*, vol. 49, no. 10, pp. 4021–4034, 2011.
- [8] P. Setlur, G. Alli, and L. Nuzzo, "Multipath Exploitation in Through-Wall Radar Imaging Via Point Spread Functions," *IEEE Transactions on Image Processing*, vol. 22, no. 12, pp. 4571–4586, 2013.
- [9] P. Setlur, T. Negishi, N. Devroye, and D. Erricolo, "Multipath Exploitation in Non-LOS Urban Synthetic Aperture Radar," *IEEE Journal of Selected Topics in Signal Processing*, vol. 8, no. 1, pp. 137–152, 2014.
- [10] G. Gennarelli and F. Soldovieri, "A Linear Inverse Scattering Algorithm for Radar Imaging in Multipath Environments," *IEEE Geoscience and Remote Sensing Letters*, vol. 10, no. 5, pp. 1085–1089, 2013.
- [11] G. E. Smith and B. G. Mobasseri, "Analysis and Exploitation of Multipath Ghosts in Radar Target Image Classification," *IEEE Transactions on Image Processing*, vol. 23, no. 4, pp. 1581–1592, 2014.
- [12] M. Leigsnering, M. Amin, F. Ahmad, and A. Zoubir, "Multipath Exploitation and Suppression for SAR Imaging of Building Interiors: An overview of recent advances," *IEEE Signal Processing Magazine*, vol. 31, no. 4, pp. 110–119, 2014.